Pflugers Arch – Eur J Physiol (2006) 451: 716–726
DOI 10.1007/s00424-005-1514-3

Guylaine M. Durand · Nima Marandi
Simone D. Herberger · Robert Blum · Arthur Konnerth

Quantitative single-cell RT-PCR and Ca^{2+} imaging in brain slices

Received: 8 June 2005 / Revised: 5 August 2005 / Accepted: 26 August 2005 / Published online: 7 October 2005

Abstract We have established a quantitative reverse transcriptase-PCR (RT-PCR) approach for the analysis of RNA transcript levels in individual cells of living brain slices. Quantification is achieved by using rapid-cycle, real-time PCR protocols and high-resolution external cDNA standard curves for the gene of interest. The method consists of several procedures, including cell soma harvest, reverse transcription, and an optimized cDNA purification step, which allowed us to quantify transcripts in small types of neurons, like cerebellar granule cells. Thus, we detected in single granule cells an average of 20 transcript copies of the housekeeping gene glyceraldehyde-3-phosphate-dehydrogenase. We combined two-photon calcium imaging and quantitative RT-PCR in single Purkinje and granule cells, respectively, and identified distinct glutamate receptor-dependent Ca^{2+} responses in these two cell types. The approach was further tested by profiling the expression of the ionotropic glutamate receptor subunits NR2B and NR2C in the cerebellum. Our study revealed a developmental switch from an average of 15 NR2B copies/cell at postnatal day 8 (P8) to about five NR2C copies/cell after P26. Taken together, our results demonstrate that the new method is rapid, highly sensitive, provides reliable results in neurons of various sizes, and can be used in combination with Ca^{2+} imaging.

Keywords Cerebellum · Glutamate receptor · Calcium imaging · Gene expression · Quantitative single cell PCR

Guylaine M. Durand and Nima Marandi contributed equally to this work.

G. M. Durand · N. Marandi · S. D. Herberger · R. Blum (✉) A. Konnerth
Institut für Physiologie, Ludwig-Maximilians-Universität, Pettenkofer Straße 12, 80336 Műnchen, Germany
E-mail: blum@lrz.uni-muenchen.de
Tel.: +49-89-218075588
Fax: +49-89-218075512

Introduction

In the brain, the levels of gene expression and their regulation determine neuronal identity, including the characteristics of synaptic responsiveness and the ability to undergo cellular plasticity [8]. The investigation of quantitative changes in cell type-specific gene expression patterns at the single-cell level can help to understand the molecular basis of physiological roles of specific cell types. Following the breakthrough of successful amplification of specific RNA transcripts from single neurons by reverse transcriptase-PCR (RT-PCR) [24] or amplified-antisense RNA procedures [7], various protocols have been developed for quantifying specific transcripts from single cells [5, 14, 16, 21, 25, 26, 35, 36]. The development of real-time PCR techniques, which allows the complete DNA amplification process to be monitored directly, simplified the quantitative analysis of even low amounts of nucleic acids greatly [15, 18, 38, 39]. However, the adaptation of real-time RT-PCR to quantitative profiling of single cells involves critical experimental steps including the RNA harvest, the RT-reaction, the purification of the resulting single cell nucleic acids and finally the PCR reaction itself [4, 26]. This report describes a complete procedure for the rapid determination of the copy numbers from single cells in brain slice preparations. Quantifiable results from multiple cells can be obtained within 4 h. Further, we demonstrate the use of the method in combination with Ca^{2+} imaging.

Materials and methods

Preparation of cerebellar slices

Cerebellar slices were prepared from brains of 8- to 30-day-old Sprague-Dawley rats as described previously [9]. After decapitation, cerebella were removed and transferred into ice-cold, sucrose-based saline (in mM: 234 sucrose, 5.3 KCl, 26 $NaHCO_3$, 1 NaH_2PO_4, 8 $MgSO_4$, 10 glucose, pH 7.4 when saturated with 95% O_2 and 5%

CO_2). Parasagittal slices (300 μm) were cut and transferred to an incubation chamber containing standard saline (in mM: 125 NaCl, 2.5 KCl, 2 $CaCl_2$, 1 $MgCl_2$, 1.25 NaH_2PO_4, 26 $NaHCO_3$, and 20 glucose saturated with 95% O_2 and 5% CO_2) at 30°C. The slices were used for a maximum of 4 h. For cell harvest the slices were placed in a recording chamber and perfused with standard saline at 30°C.

Rapid cell harvest

Cerebellar granule and Purkinje cells were identified visually using an upright microscope (Axioscope FS, Zeiss, Jena, Germany) equipped with a 60× objective (Olympus, Tokyo, Japan) and an infrared sensitive video camera (C2400, Hamamatsu, Japan). For cell harvest, standard patch-clamp pipettes were made from borosilicate glass (2.0/0.3 mm; Hilgenberg, Malsfeld, Germany) using a Narishige PC-10 pipette puller. Using a double-pull routine, tip diameters of about one-third of the cell soma diameter (8 μm for Purkinje cells and 3 μm for granule cells) were produced by modifying the heat of the second pulling step. The pipette solution (RNA protecting solution: RPS) consisted of 4 μl H_2O with 15 U RNAse-inhibitor (Promega, Mannheim, Germany), 25 mM DTT. A pipette was moved into the bath solution under positive pressure (100 Pa) to avoid aspiration of extracellular solution. As the pipette tip approached the selected neuron, the pressure in the pipette was released to prevent cell swelling or bursting induced by the pipette solution. Under visual control, the tip of the pipette was gently attached to the selected cell. Through a mouthpiece connected to the pipette, suction was applied, until the cell entered the tip of the pipette (Fig. 1a). As soon as the complete cell had been located within the tip, the negative pressure was released to minimize the collection of extracellular solution. The pipette was removed quickly from the bath. Pooled granule cells were collected subsequently into the same pipette and accumulated together in the very tip of the pipette.

Reverse transcription

Under a dissecting microscope, the content of the pipette was pressure-ejected (N_2, 200–400 kPa) into a PCR tube containing 2 μl nucleotide/detergent solution 10 mM Tris–HCl, pH 8.0, 25 μM random hexamers (Roche, Mannheim, Germany), 2.5 mM of each dNTP (Amersham-Pharmacia, Freiburg, Germany), 0.2% Nonidet P40 (Roche)], denatured at 70°C for 5 min and placed on ice for about 5 min. Then 2 μl of 5× First-strand buffer (Invitrogen, Karlsrube, Germany), 0.5 μl of 200 mM DTT, 20 U RNAse-inhibitor (Promega) and 100 U Moloney murine leukaemia virus reverse transcriptase (Invitrogen) were added. The RT reaction (final volume: 10 μl) was incubated at 37°C for 1 h and stopped at 95°C for 5 min. As negative controls, the RT reactions were performed in the absence of either RNA or reverse transcriptase. Furthermore, standard saline collected with a glass pipette from the extracellular slice environment was tested routinely.

cDNA purification

For cDNA purification, the QIAEX II gel extraction Kit (Qiagen, Hilden, Germany) was used. The complete RT-reaction (10 μl) was mixed with 80 μl QX1 binding buffer and 1.5 μl DNA-binding matrix per RT reaction at 25°C for 15 min in a thermomixer (Eppendorf, Hamburg, Germany) at 1,400×*g*. The binding matrix was pelleted (13,000×*g*, 2 min) and washed twice in 90 μl ice-cold, ethanol-based PE-buffer (Qiagen). The DNA-binding matrix was dried at 37°C for 10 min to remove the ethanol completely. Finally, the cDNA was eluted with an appropriate volume (> 5 μl) of 1 mM Tris-HCl, pH 8.5 at 50°C for 3 min. After purification, it was possible to store the cDNA material, together with the binding matrix, at −70°C. Before use, the binding matrix was pelleted (13,000×*g*, 2 min) and the supernatant was directly used for the real-time PCR analysis. Note that it is critical that the supernatant is totally free of binding matrix.

Primer selection

Primers were selected using the Oligo 6.0 primer analysis software (MedProbe, Oslo, Norway). Briefly, the following primer parameters were found to give best results: selection of intron-spanning primers, when possible; primer length: 17–21 bp; 3′-terminal dimer formation: < (−3.0) kcal/mol; optimal annealing temperature: 58–65°C; amplicon length: 100–250 bp; product melting temperature: 85–91°C; G/C-content: 45–60%; high internal stability at the 5′-end and medium internal stability at the 3′-priming site; minimal acceptable loop (hairpin formation) at the 3′-end: 0.0 kcal/mol; maximum length of acceptable dimers (5′-end/internal region): 4 bp. The primer pairs for NR2B, NR2C and GAPDH were tested for high sensitivity (detection of one to two double-strand standard copies). Since primer dimers act as competitive inhibitors of PCR, we verified that no primer dimers appeared in the presence of small amounts of cDNA from RT reactions of cerebellar total RNA (500 fg–10 pg). Using isolated rat genomic DNA as control, we ensured that genomic DNA did not contribute to the RT-PCR products of GluRδ2, NR2B, and NR2C.

Rapid-cycle, real-time PCR

The cDNAs encoding GAPDH, NR2B, NR2C, and GluRδ2 were amplified using specific primers (MWG Biotech, Ebersberg, Germany, Table 1). PCR was per-

formed in a volume of 20 µl including 2 µl 10× DNA Master SYBR-Green mix (Roche). To ensure 'hot start conditions', the SYBR-Green mix was pre-incubated with 0.16 µl/reaction Taq Start antibody (Clontech, Heidelberg, Germany) for 5 min at room temperature. PCRs were optimized for (in order): magnesium concentration, primer concentration, annealing temperature, and the product specificity temperature, at which the specific products melt (Table 2). PCR products were verified with both melting curve analysis and DNA gel electrophoresis. In some cases, PCR products of single cells were analyzed by DNA sequencing. For very small amounts of cDNA, it was important to analyze not more than 12 samples per Lightcycler run. We found that simultaneous analysis of more than 12 samples per run reduced the efficiency of the PCR. Most likely, the time the Lightcycler device needs to read each sample before the run and also the time for the real-time measurements of individual samples during the run, both affect PCR performance. Before the next PCR run, it was necessary to cool the thermal chamber of the Lightcycler to room temperature (21–23°C). In our protocol, the use of the Taq Start antibody was an absolute necessity for the detection of low copy numbers.

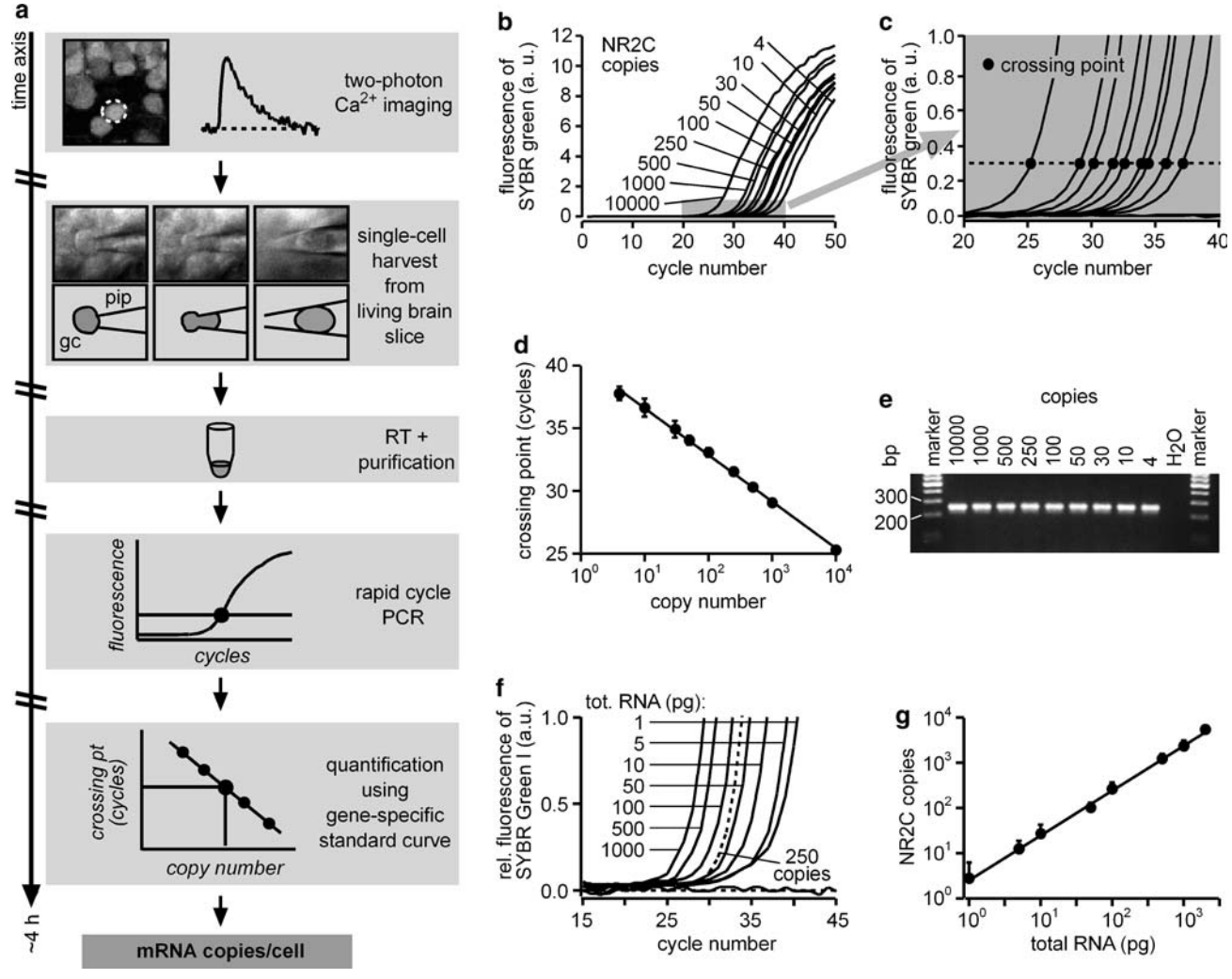

Fig. 1 **a**–**g** Single-cell, real-time PCR from acute brain slices. **a** Illustration of the experimental procedure. *RPS*, RNA protecting solution. **b** PCR calibration with NR2C amplicons. Real-time monitoring of the fluorescence emission of SYBR Green I during the PCR amplification of defined amounts of NR2C amplicons (serial dilutions containing 4–10,000 copies in this example). The small *gray rectangle* is enlarged in **c**. **c** Fluorescence monitoring of the PCR amplification of the NR2C amplicon solutions shown in **b** during the exponential phase of the PCR. At a gene-specific fluorescence value (*dashed line*; calculated to represent 4.6×10^{11} NR2C copies), the crossing point is determined. **d** Standard curve of the NR2C amplicon serial dilutions. Individual *data points* represent mean ± SEM of ten samples of equal amounts of NR2C amplicon copies. **e** Agarose gel electrophoresis of PCR products obtained in **b** after 50 cycles of PCR amplification. The size of the NR2C amplicon is 255 bp. **f** NR2C-specific RT-PCR of defined amounts of total RNA after purification and RT (serial dilutions containing 1–2,000 pg total RNA). **g** Correlation between the amount of total RNA and the number of NR2C copies are determined by the NR2C standard curve. Individual data points represent means ± SEM of ten samples. The *line* represents the regression of the data points

Table 1 Primers

Gene	Accession	Forward primer/reverse primer	Length (bp)	Intron-spanning
NR2C	U08259	1502-for 5′-CTGGGGACTGCCGAAGMCAC-3′ 1756-rev 5′-CCACCACAGGCTGCAGAGAA-3′	255	Yes
NR2B	U11419	2887-for 5′-TCCGGCATTGCTTCATGGGT-3′ 2994-rev 5′-ATTGGCGCTCCTCTATGGCT-3′	108	Yes
GAPDH	X02231	226-for 5′GCAAGTTCAACGGCACA-3′ 366-rev 5′CGCCAGTAGACTCCACGAC-3′	141	No
GluRδ2	U08256	2172-for 5′GGGGAAGTACCATACACAAC-3′ 2887-rev 5′TTCCGCCGACTCCACCATGT-3′	716	Yes

Table 2 Optimized parameters of real-time PCR using the lightcycler

Gene	[$MgCl_2$] (mM)	[primer] (μM)	$T_{denat.}$, time	$T_{annealing.}$, time	$T_{extension}$, time	$T_{product\ specificity}$, time
NR2C	4	1.0	95°C, 0 s	65°C, 5 s	72°C, 11 s	88°C, 5 s
NR2B	3	1.5	95°C, 0 s	59°C, 5 s	72°C, 5 s	84°C, 5 s
GAPDH	4	1.5	95°C, 0 s	59°C, 5 s	72°C, 5 s	85°C, 5 s
GluRδ2	6	1.0	95°C, 0 s	55°C, 5 s	72°C, 30 s	83°C, 10 s

Quantification with gene-specific standard curves

Unknown copy numbers were determined from gene-specific external standard curves. The cDNA standards were prepared from plasmids containing cDNA inserts for rat GAPDH, NR2B, NR2C, and GluRδ2. The inserts of these plasmids were cut and purified and used in subunit-specific, real-time PCR. The resulting PCR products were purified, analyzed, and quantified photometrically at 260 nm (Genequant, Amersham Pharmacia). The molecular weight of the cDNA templates was calculated using the Nucweight algorithm of the Husar sequence analysis software (DKFZ, Heidelberg, Germany). Quantified cDNA was diluted from 10^{10} to 2 copies per reaction in 16 steps (two copies is equivalent to one double-strand cDNA copy) and put into reaction tubes pre-coated with 10 mM Tris-HCl, pH 8.5, and 1 mg/ml purified BSA (New England Biolabs, Frankfurt, Germany). The cDNA standards were stored in a volume of 100–200 μl at −20°C and used to create external standard curves. Quantification of the samples was performed as described by Rasmussen [33]. Total RNA was prepared by standard protocols and quantified at 260 nm.

Ca^{2+} imaging and pharmacology

Fluorometric two-photon Ca^{2+} measurements [6] were performed as described previously [10, 13] except that Fura PE3 AM (TEF LABS, Austin, TX, USA) was used instead of Fura-2 AM, because Fura PE3 resists rapid leakage [37]. Glutamate (100 mM) and NMDA (10 mM) were applied iontophoretically (MVCS-02, npi, Tamm, Germany) from a fine glass pipette (20–30 MΩ, borosilicate, Hilgenberg, Germany) for 60–100 ms with retaining and ejection currents of 2 and 60–70 nA, respectively. For pharmacological experiments, we used Mg^{2+}-free saline (see above, standard saline without $MgCl_2$) containing 10 μM bicuculline, 10 μM glycine, and 500 nM TTX (Alomone, Jerusalem, Israel); CNQX (10 μM) was added in NMDA application experiments. Drugs were purchased from Sigma (Deisenhofen, Germany) unless indicated otherwise.

Results

Figure 1a depicts the individual steps of the quantitative RT-PCR approach. First, cells from an acute brain slice preparation [9] are characterized functionally using the two-photon Ca^{2+}-imaging method. Cells of interest are harvested using wide-tipped glass pipettes and the content of the pipette is pressure-ejected into a PCR tube containing a nucleotide/detergent solution to rupture the cell membrane. Then, a standard RT reaction using random hexamers is performed. Since some components of the RT-reaction may strongly decrease the PCR efficiency, we established a rapid procedure for purifying even small amounts of cDNA. Real-time monitoring of PCR kinetics is then performed using the Lightcycler (Roche) [39]. Finally, mRNA levels in single cells are quantified precisely using previously established transcript-specific, high-resolution external standard curves.

To test our single-cell RT-PCR approach, glyceraldehyde-3-phosphate-dehydrogenase (GAPDH) was employed as a ‘housekeeping’ gene. We then analyzed the ionotropic glutamate receptors/subunits NR2B, NR2C, and GluRδ2 in the rat cerebellum. In this brain region, Purkinje cells express the ionotropic glutamate receptor protein GluRδ2 selectively [20], but lack the NMDA receptor subunits NR2B and NR2C. In contrast, granule cells do not express GluRδ2, but show a developmental switch from NR2B to NR2C expression [11, 29].

Table 3 Characteristics of the external standard curves

Gene	Mean slope	*Y*-intercept	Efficiency	Regression
NR2C	−3.72	40.32	1.86	0.998
NR2B	−3.37	36.51	1.98	0.999
GAPDH	−3.44	35.99	1.98	0.999
GluRδ2	−3.52	41.08	1.92	0.999

High-resolution external standard curves

For the calculation of the absolute amount of transcripts in a given sample, high-resolution external standard curves were developed. For the construction of these standard curves, PCR-products of rat GAPDH, NR2B, NR2C, and GluRδ2 were quantified at 260 nm, serially diluted (10^{10} to 2 calculated single-strand copies) and used subsequently for the real-time PCR (representatively explained for NR2C, Fig. 1b–e). A constant threshold fluorescence value that represented equal synthesized DNA amounts from each dilution (Fig. 1c, see dashed line, calculated to represent 4.6×10^{11} NR2C copies), was selected from the exponential phase of the PCR. To construct the external standard curve, the cycle number at this threshold band (the so-called crossing point, CP [33]), was plotted as a function of the logarithm of the standard copy number for each of the serial dilutions (Fig. 1d). The CPs of the different dilutions were proportional to the logarithm of the copy numbers from 10^4 to 4 single-stranded cDNA copies. Even as few as two NR2C copies (one double-strand DNA copy) were detectable in 25% of all experiments performed ($n=20$). The characteristics of the external standard

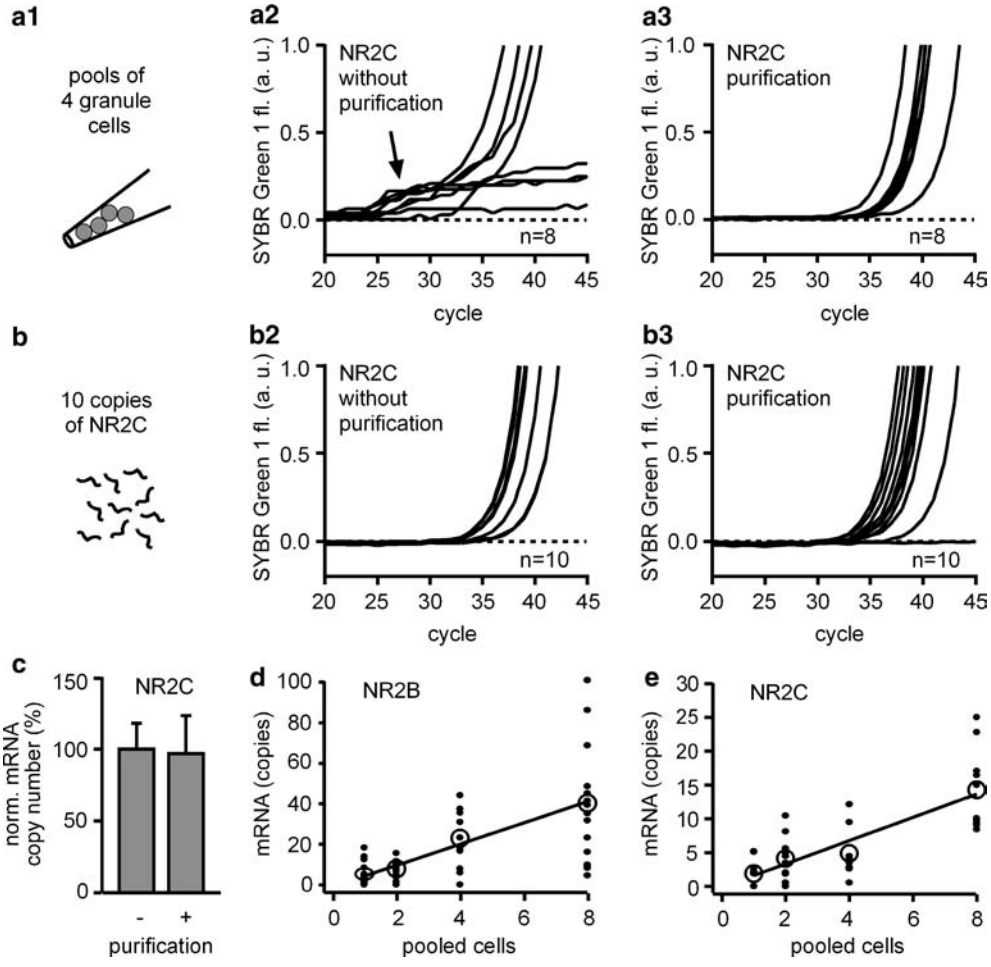

Fig. 2 a–e Rapid quantitative purification of small amounts of cDNA. **a** NR2C-specific RT-PCR of pools of four cerebellar granule cells **a1** without **a2** and with **a3** a DNA purification step after the RT. Note the hump **a2** (*arrow*) before the exponential phase and the high failure rate (four out of eight) in the samples without purification. **b** NR2C-specific RT-PCR of samples containing ten copies of NR2C DNA amplicons without **b2** and with **b3** purification. **c** Relative number of NR2C copies from the samples in **b**. NR2C copy numbers of purified samples are normalized by reference to the mean copy number of unpurified samples. A mean (±SEM) yield of 97±26.5%, $n=10$) of ten initial NR2C copies was rescued by the cDNA-purification method. **d, e** Correlation between the size of granule cell pools and the number of mRNA copies for NR2B **d** and NR2C **e**. *Small dots* indicate results from individual samples. Large circles indicate average copy numbers for each pool size. The *line* describes the regression of all data points

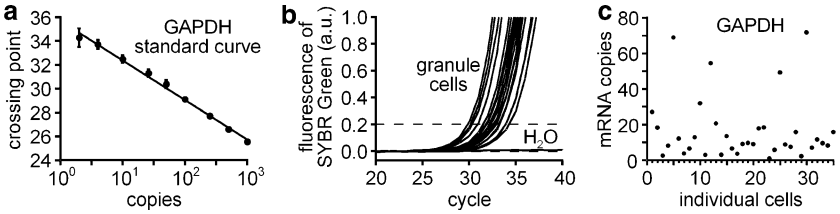

Fig. 3 a–c Quantitative single-cell RT-PCR of a housekeeping gene. **a** Standard curve made with serial dilutions of the glyceraldehyde-3-phosphate-dehydrogenase (GAPDH) amplicon. Individual *points* represent means ± SEM; $n = 10$ samples. For standard curve characteristics see Table 3. **b** Real-time monitoring of the fluorescence emission of SYBR Green I during the PCR amplification of GAPDH. As template, purified cDNA from single cerebellar granule cells was used ($n = 36$). H_2O was used as a negative control. **c** Variation of GAPDH mRNA expression in individual cerebellar granule cells

curves for NR2C, NR2B, GAPDH, and GluRδ2 are listed in Table 3. The expected size of all PCR products was verified by gel electrophoresis (here shown for NR2C, Fig. 1e).

Efficiency of reverse transcription

Quantitative amplification of a single stranded cDNA template requires the efficient binding of the forward primer in early phases of the cycle. To monitor RT reproducibility with low target amounts, we quantified NR2C transcripts from dilution series of total cerebellar RNA. The RNA was diluted in seven steps from 2 ng to 0.01 pg, and ten separate RT reactions were performed for each dilution. Figure 1f illustrates representative fluorescence data resulting from NR2C amplification after RT. The NR2C copy numbers in serially diluted total RNA were determined using the external NR2C standard curve (Fig. 1d). A plot of the RNA amount as a function of the NR2C copy number shows a linear correlation (Fig. 1 g; ms: 3.43, $E = 1.96$, $r = 0.993$). Below 500 fg RNA entry material, representing a calculated average of about one NR2C copy, no amplification was observed. In summary, the RT-reaction gives highly reproducible results.

Rapid cell harvest

The harvest of RNA from living single cells has been performed previously by aspiration of the cytosolic material into the recording patch-clamp pipettes [7, 19, 24, 25, 32, 35]. Our new approach consisted of gentle aspiration of a visually identified, single neuronal soma into the tip of a glass pipette filled previously with 4 µl RNA-protecting solution, consisting of water, 25 mM DTT and 15 U RNAse-inhibitor/cell. To ensure that the complete cellular RNA was expelled into a RT-reaction tube as quickly as possible, the content of the pipette

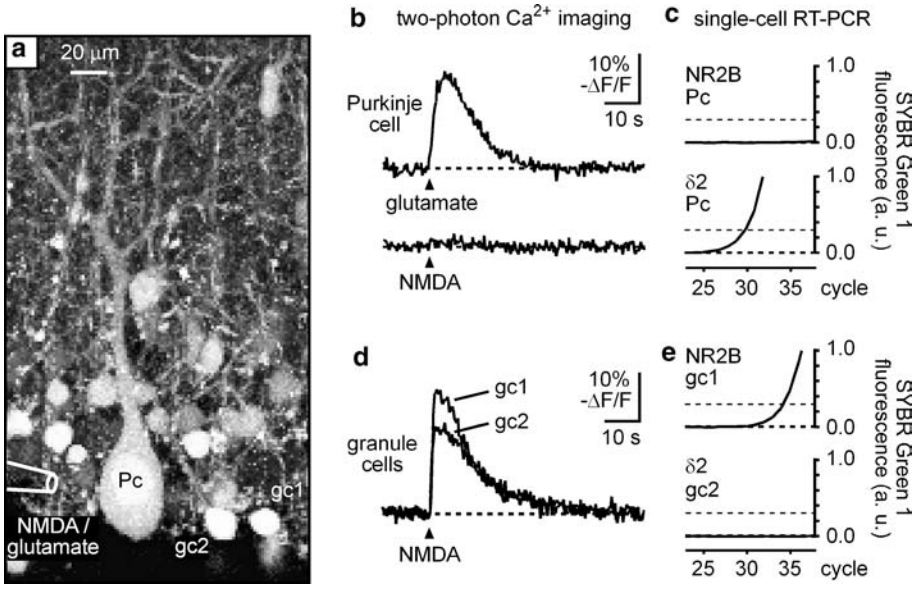

Fig. 4 a–e Combination of Ca^{2+} imaging and single-cell RT-PCR in acute brain slices. **a** Two-photon fluorescence image of a cerebellar slice from a 12-day-old rat, loaded with the Ca^{2+} indicator dye Fura PE3 AM. From a pipette, NMDA or glutamate was applied iontophoretically on the somata of a Purkinje cell (*Pc*) and two granule cells (*gc*1, *gc*2). **b** Ca^{2+} responses evoked by brief applications of glutamate and NMDA on the Purkinje cell shown in **a**. **c** NR2B- and GluRδ2-specific RT-PCR in both halves of the Purkinje cell. **d** Ca^{2+} responses evoked by brief applications of NMDA on the granule cells shown in **a**. **e** NR2B- and GluRδ2-specific RT-PCR of the granule cells *gc*1 and *gc*2

was pressure-ejected (N_2, 200–400 kPa). For example, the harvest of a small cerebellar granule cell (Fig. 4a) was usually achieved within less than 20 s. The harvest procedure of a Purkinje cell (Fig. 4a) lasted for about 1 min. This included the time needed to detach the soma from the largely ramified dendrites and the axon.

Rapid purification of cDNA from single cel RT reactions

Components of the RT reaction, including the reverse transcriptase itself, substantially decrease PCR efficiency [4, 26]. When we attempted to detect NR2C transcripts directly from single granule cells, which functionally express this glutamate receptor subunit [11, 29], the experiments failed. We therefore pooled four single granule cells in one harvesting pipette and repeated the RT-PCR. As shown in Fig. 2a1, some pools of four cells gave a positive result, but in contrast to RT-PCRs from total RNA, the amplification kinetics varied from sample to sample, impeding the quantification of the samples (see arrow in Fig. 2a2). To overcome this problem, it was necessary to establish a rapid procedure for the purification of cDNA from single cell RT reactions. We used a commercially available DNA-binding matrix (Qiagen) in a batch purification procedure. To ensure that this step was quantitative, we purified ten copies of NR2C standard DNA and subsequently verified with quantitative PCR that these ten copies were indeed recovered by the DNA purification procedure [Fig. 2b, c; mean (±SEM) recovery 97% ± 26.5 of ten copies, $n = 10$]. The quantitative analysis of NR2C from pooled granule cells was now feasible and all samples showed regular PCR kinetics (Fig. 2a3). Within our previous study [16], we confirmed the accuracy of the purification method using 1,000 standard cDNA copies for $G\alpha_q$, and ten copies for $G\alpha_{11}$ (not shown).

Correlation between cell number and copy number

To establish that the cell harvest method and the downstream procedures are constant, we collected one, two, four or eight cerebellar granule cells in a single glass pipette and determined the number of NR2C and NR2B copies. As shown in Fig. 2d, e, the number of detected transcript copies was proportional to the number of collected cells, even with very low copy numbers (means ± SEM, NR2B: one cell = 3.9 ± 1.7 copies; eight cells 42.5 ± 14.3 copies; NR2C: one cell = 2.1 ± 0.8 copies, eight cells = 14.3 ± 1.9 copies; $n = 7$) (NR2B, linear

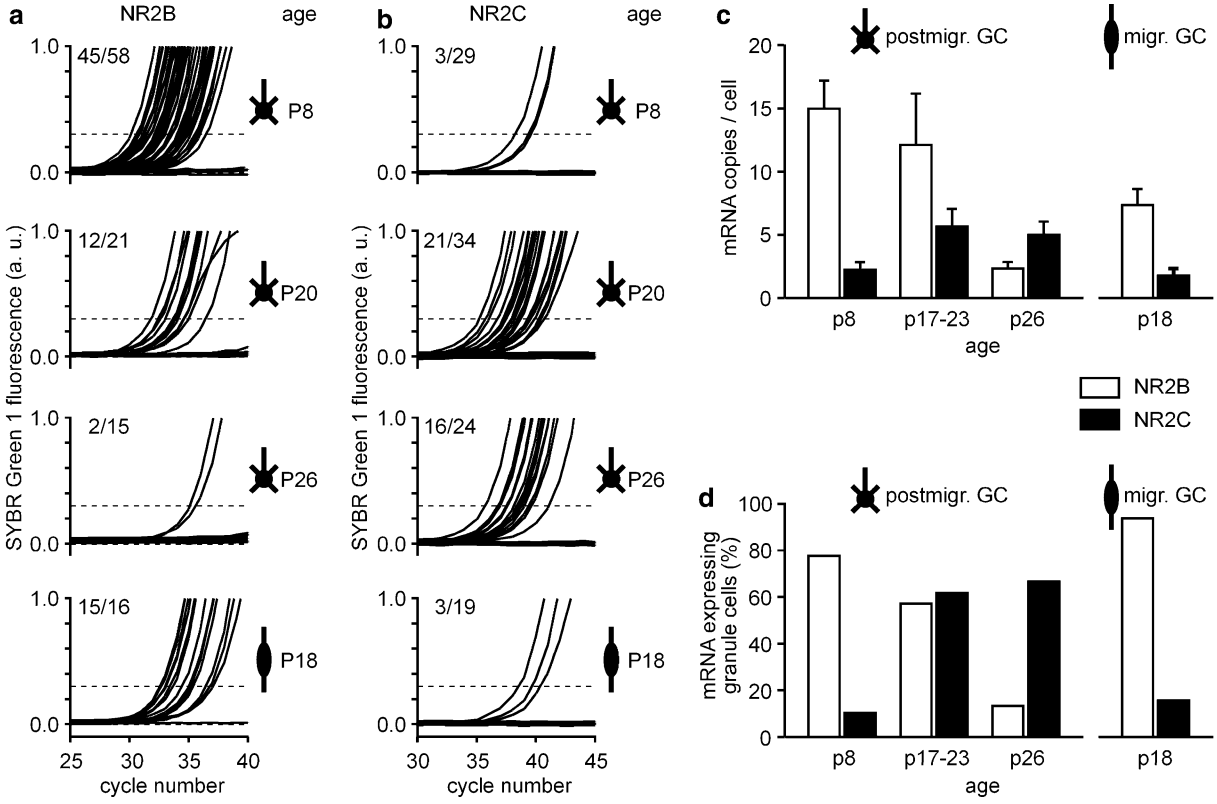

Fig. 5 a–d Developmental switch of mRNA encoding NMDA receptor subunits. **a, b** Real-time monitoring of NR2B- **a** and NR2C- **b** specific RT-PCR as analyzed in **c, d**. As template, purified cDNA from single cerebellar granule cells was used. **c** Average NR2B and NR2C mRNA expression levels in single granule cells during development. Developmental stages and ages of the animals are indicated. **d** Percentage of granule cells containing mRNA for NR2B and NR2C during development. *Round cells with small processes*, postmigratory granule cells in the internal granule cell layer; *spindle shaped cells with axial processes*, migrating granule cells

regression: $r = 0.672$, $P < 0.0001$, mean slope = 5.27; NR2C, linear regression: $r = 0.761$, $P < 0.0001$, $ms = 1.72$).

Quantitative single cell RT-PCR of a housekeeping gene

Glyceraldehyde-3-phosphate-dehydrogenase is a housekeeping gene, the transcripts of which are localized exclusively in the cell soma [27]. To test the success rate of our RNA harvest procedure and cDNA purification step, we determined GAPDH copy numbers in individual cerebellar granule cells. The mean (±SEM) copy number was 20.3 ± 4.5 ($n = 36$) per cell. The detection of the housekeeping gene never failed, but the copy number of GAPDH varied considerably from cell to cell (Fig. 3). There was no false positive amplification of GAPDH in control reactions without reverse transcriptase, despite the fact that primers used for GAPDH amplification were not intron-spanning.

Quantitative single-cell RT-PCR and Ca^{2+} imaging in acute brain slices

Next, we combined two-photon Ca^{2+} imaging with single-cell quantitative RT-PCR in acute cerebellar slices. For this purpose, we tested the function and the expression of cell type-specific glutamate receptors in the cerebellum. The GluRδ2 subunit of the glutamate receptor family is expressed selectively in Purkinje cells and plays important roles in synapse formation and synaptic plasticity [20]. Analysis of the mean (±SEM) expression level of GluRδ2 transcripts in Purkinje cells (P14) yielded 13,360 ± 1,595 copies/half cell ($n = 24$) (about 27,000 copies per Purkinje cell).

In contrast, the NR2B subunit of the NMDA glutamate receptor is expressed in immature cerebellar granule cells but not in Purkinje cells [1]. Figure 4a illustrates a Purkinje cell and two granule cells in the cerebellar cortex of an acute brain slice from a 12-day-old rat, loaded with the membrane-permeable Ca^{2+} indicator dye Fura PE3 AM. The application of NMDA evoked Ca^{2+} signals in the granule cells (Fig. 4d) but not in Purkinje cells (Fig. 4b), consistent with the finding that Purkinje cells do not express functional NMDA receptors at this developmental stage [17]. The viability of the Purkinje cell in this experiment was proved by a glutamate induced Ca^{2+} signal (Fig. 4b). After harvest of this Purkinje cell and reverse transcription of its RNA, we divided this RT material in two equal portions and analyzed them for the presence of GluRδ2 and NR2B mRNA, respectively (Fig. 4c). GluRδ2 (4,272 copies/half cell), but no NR2B transcripts were detected in the other half of this Purkinje cell. In the case of granule cells, due to their low expression level of NR2B, RT material from two whole cells was compared. In contrast to the Purkinje cell, one granule cell did not express GluRδ2 (gc2, Fig. 4a, e), while the other granule cell (gc1, Fig. 4a, e) expressed NR2B (five copies). It is important to stress that our effective purification procedure removed all traces of the fluorometric Ca^{2+} indicator (Fura PE3 AM) allowing an accurate fluorometric monitoring (SYBR green I) of the PCR, as demonstrated, for example, by the similarity of the NR2B transcript numbers in stained (Fig. 4e) and non-stained granule cells (Fig. 5c).

Developmental switch of NR2-subunit mRNA in cerebellar granule cells

We tested the new RT-PCR approach by analyzing the well-established developmental NMDA receptor switch [11, 29] in rat cerebellar granule cells. For this purpose, single cerebellar granule cells from the internal granule cell layer were analyzed at P8, P17–P23, and P26 (Fig. 5). In young rats, at P8, 45 out of 58 granule cells expressed a mean (±SEM) number of NR2B copies of 15.0 ± 2.2 per cell. In contrast, only three out of 29 cells expressed NR2C. These positive cells contained about two copies per cell (mean 2.2 copies).

In juvenile rats (P17–P23), 21 out of 34 granule cells were positive for NR2C (5.6 ± 1.4 copies per cell), while 12 out of 21 cells contained NR2B (12.1 ± 4.0 copies per cell). In older rats, at P26, the developmental switch from NR2B to NR2C was nearly complete. Most cells were NR2C-positive (NR2C: 16 out of 24; 5.0 ± 1.0 copies) while only a minor fraction of cells expressed NR2B (two out of 15 cells positive; 2.3 copies per positive cell).

These results reveal two different alterations, both of which contribute to the NR2 subunit switch: (1) changes in cell numbers expressing either NR2B or NR2C and (2) changes in expression levels of these subunits in individual cells. For example, at P8, the majority of cells express NR2B. At P17–P23, the percentage of cells expressing NR2B decreases, but NR2B copy numbers in these single cells remain constant. Later in development, at P26, NR2B was detected only in very few cells and at much lower levels.

In contrast to mature granule cells, migrating granule cells represent a developmentally immature state [23]. As shown in Fig. 5, at P18, migrating granule cells preferentially express NR2B (15 out of 16 positive with 7.34 ± 1.3 copies per cell) while NR2C was detected in only 3 out of 19 cells (mean 1.8 copies).

Discussion

Here, we describe a fast and highly sensitive method for determining absolute RNA copy numbers in single neurons from acute brain slices. Importantly, the method can be combined with single-cell functional analysis involving fluorometric Ca^{2+} imaging.

RNA harvest and reverse transcription from single cells

Various methods to harvest RNA material from single cells have been described so far. Sophisticated devices to collect single cell RNA, such as laser assisted cell picking systems [12] or atomic force microscopes [30], are either unsuitable for use in living tissues or can harvest only a fraction of the total cellular content, respectively. Pioneering studies described the collection of RNA from single neurons by aspiration of the cytosol into micropipettes, immediately after a session of patch-clamp recordings [7, 19, 24]. This method, which was also adopted in our laboratory [32], has become a powerful tool for the investigation of the molecular basis of cellular function. However, in our experience it was very difficult to collect the intracellular, somatic RNA content in reproducible amounts. Therefore, we decided to aspirate complete neuronal somata of living neurons into wide-opened glass pipettes filled with a RNA-protecting solution and used the complete somatic content for RT-PCR analysis. Neighboring cells were left intact, thus minimizing the risk of RNA contamination. An important advance was the use of the RNA-protecting solution for the collection of single cells. This solution allows the reverse transcription reaction to be performed under optimal buffer conditions. When analyzing the results obtained with our aspiration method, it is important to consider the possibility of the presence of presynaptic endings attached to the somatic membrane, and, thus, a contamination with presynaptic mRNA [31].

cDNA purification of single cell RT material

The direct use of single-cell RT reactions in real-time, rapid-cycle PCR reduced the amplification efficiency (Fig. 2a2). This necessitated a method for the efficient purification of cDNA from single cells. We tested various protocols including phenol/chloroform extraction, ethanol precipitation, and gel filtration chromatography, but none of these were able to purify the single-cell samples without significant cDNA loss. Finally, we were able to reliably recover low amounts of cDNA from single cells using DNA-binding matrix. Recently, Liss [26] described a quantitative single cell cDNA purification protocol-based on carrier-assisted ethanol precipitation. The advantages of the protocol used here are its speed, simplicity, and the low risk of losing the single-cell cDNA sample during purification.

Reliability of single-cell RT-PCR and the normalization of expression levels

The applicability of all our experimental procedures for the analysis of gene expression levels in single cells was tested by investigating the abundance of the housekeeping gene GAPDH in cerebellar granule cells. Of 36 single cells tested, all were positive for GAPDH, meaning that the cell harvest procedure and all subsequent steps were performed with a reliability of 100%. For quantification of GluRδ2 transcripts in cerebellar Purkinje cells, a different transcript and cell type, a success rate of 100% ($n = 24$) was also achieved. Alternative RNA harvest methods, e.g. the laser-assisted cell picking method (82% success rate with the housekeeping gene porphobilinogen deaminase) [12] or atomic force microscope assisted RNA picking (96.3% positive cells with actin transcripts) [30] are somewhat less efficient than the present approach.

The identification of a valid reference for data normalization remains a major problem in quantitative analysis of gene expression. Housekeeping genes such as β-actin or GAPDH are used commonly as standards for the normalization of global quantification data [3, 33]. In contrast, for single cell analysis, continuing reports [3, 25, 30], as well as this study (Fig. 3), emphasize the problems arising from the use of housekeeping genes as denominators, due to considerable variation in the expression level between individual cells. We therefore decided to calculate the absolute copy number of each transcript per cell, using transcript-specific external standard data obtained with the same procedure.

Cellular imaging and gene expression analysis in single cells

The combination of imaging techniques with quantitative single-cell RT-PCR opens the possibility for combined functional-molecular analysis in multicellular networks. In contrast to patch-clamp recordings [7, 24, 25, 32], imaging techniques allow the simultaneous analysis of tens of cells, instead of only one, and allow an easier experimental access to mechanisms in which intracellular signaling cascades play an important role. On the other hand, the combination of patch-clamp recordings with single-cell PCR techniques is particularly useful, when the electrophysiological characterization of specific membrane parameters, like specific features of ion channel function, are important to define the molecule-function relation. For the imaging analysis of cells in slice preparations, it is recommended, but not always mandatory, to use two-photon imaging [6] to avoid contamination by signaling from neighboring cells. Many of the standard fluorometric indicators are usable with two-photon imaging. These include those for the monitoring of Ca^{2+} ions [2, 10, 13], Na^{+} ions [34] and Cl^{-} ions [28].

High-resolution, quantitative, single-cell RT-PCR in gene expression profiling

As a test of our method, we analyzed a well-described developmental switch in the expression of NMDA receptor subunits in rat cerebellar granule cells [11, 29].

In early development, granule cells preferentially express NR2B. After P12, the expression level of NR2B gradually decreases and is replaced by NR2C, the predominant NR2 subunit of NMDA receptors in mature granule cells [11, 29]. Our results not only reflect this developmental process (see Fig. 5), but also reveal new properties of this switch. Changes in cell numbers expressing either NR2B and/or NR2C and changes in the expression levels of these subunits in individual cells, both contribute to the NR2 subunit expression profile. Migrating granule cells in the molecular layer represent an early stage in their cellular development [22]. Accordingly, we observed the preferential expression of NR2B in single migrating granule cells at P18. This reveals an additional aspect of NR2B as a marker for immature or migrating granule cells, regardless of the animal's chronological age.

Quantification limits

The accuracy of quantification is determined by (1) the harvest procedure (see above) and (2) the efficiency of the reverse transcription of cellular RNA. We found that the use of random hexamers is consistently more reliable and effective than the use of polyT-primers (data not shown). The use of Superscript II did not provide better results. (3) In principle, also the purification procedure needs to be considered. Our results indicate, however, that our approach works particularly accurate, without evidence for a substantial loss (see above). (4) Finally, a critical factor for quantification is the use of external standards. Only very few cycles of a PCR can in fact be described by an exponential growth curve [33]. Therefore, as a prerequisite for the quantification of low amounts of transcripts (from 100 copies down to one copy), we established high-resolution external standard curves, which describe statistically each gene-specific quantitative PCR in its critical phase with multiple data points (100, 50, 26, 10, and 4 copies). As the actual quantification limit of a given standard cDNA always depended on the chosen primers and product sequence, we tested multiple primer pairs for NR2B, NR2C, and GAPDH, until the reproducible quantification of a minimum of four copies (two double-stranded DNA copies) was possible and described by the regression line of the high-resolution standard curve (at least 90% positive runs for ten copies or five double-stranded DNA copies; $>50\%$ positive runs for four copies or two double-stranded DNA copies). Real-time PCR quantifications in the range of one to four copies, when the random variation due to sampling error (called Poisson error) becomes significant [33], represent the theoretical limit of quantification. Thus, it was quite challenging to quantify in the small granule cells the expression levels for NR2B, NR2C, or GAPDH, which were, in some experiments, found to be below four copies. In this case (below four copies), we estimated the copy numbers by the regression line of the standard curve. The reproducibility of reverse transcription, even of low RNA amounts (see Fig. 1g), and the exact definition of the quantification limit for each target, together justify the use of high-resolution external double-stranded DNA standards for the quantification of low levels of RNA transcripts.

Conclusion

In this study we report a new Ca^{2+}-imaging/single cell RT-PCR approach. Our protocol includes (1) the harvest of defined living neurons, (2) an effective purification approach of single-cell cDNA, (3) a sensitive expression analysis, and (4) fast, combined functional-molecular analyses on the single cell level. At present, this method is one of the most sensitive and efficient approaches for functional-molecular analysis in multicellular networks.

Acknowledgments We thank Dr. Alexandra Lepier and Dr. John Davis for comments on earlier versions of the manuscript and I. Mühlhahn for technical assistance. The work was supported by grants from the DFG and the BMBF. *Competing interests statement*: The authors declare that they have no competing financial interests. This study was not financially supported by the companies selling reagents or instrumentation used in this approach.

References

1. Akazawa C, Shigemoto R, Bessho Y, Nakanishi S, Mizuno N (1994) Differential expression of five N-methyl-D-aspartate receptor subunit mRNAs in the cerebellum of developing and adult rats. J Comp Neurol 347:150–160
2. Brustein E, Marandi N, Kovalchuk Y, Drapeau P, Konnerth A (2003) "In vivo" monitoring of neuronal network activity in zebrafish by two-photon Ca^{2+} imaging. Pflügers Arch 446:766–773
3. Bustin SA (2002) Quantification of mRNA using real-time reverse transcription PCR (RT-PCR): trends and problems. J Mol Endocrinol 29:23–39
4. Chandler DP, Wagnon CA, Bolton H Jr (1998) Reverse transcriptase (RT) inhibition of PCR at low concentrations of template and its implications for quantitative RT-PCR. Appl Environ Microbiol 64:669–677
5. Chow N, Cox C, Callahan LM, Weimer JM, Guo L, Coleman PD (1998) Expression profiles of multiple genes in single neurons of Alzheimer's disease. Proc Natl Acad Sci USA 95:9620–9625
6. Denk W, Strickler JH, Webb WW (1990) Two-photon laser scanning fluorescence microscopy. Science 248:73–76
7. Eberwine J, Yeh H, Miyashiro K, Cao Y, Nair S, Finnell R, Zettel M, Coleman P (1992) Analysis of gene expression in single live neurons. Proc Natl Acad Sci USA 89:3010–3014
8. Eberwine J (2001) Single-cell molecular biology. Nat Neurosci 4(Suppl):1155–1156
9. Edwards FA, Konnerth A, Sakmann B, Takahashi T (1989) A thin slice preparation for patch clamp recordings from neurones of the mammalian central nervous system. Pflügers Arch 414:600–612
10. Eilers J, Plant TD, Marandi N, Konnerth A (2001) GABA-mediated Ca^{2+} signalling in developing rat cerebellar Purkinje neurones. J Physiol 536:429–437
11. Farrant M, Feldmeyer D, Takahashi T, Cull-Candy SG (1994) NMDA-receptor channel diversity in the developing cerebellum. Nature 368:335–339

12. Fink L, Seeger W, Ermert L, Hanze J, Stahl U, Grimminger F, Kummer W, Bohle RM (1998) Real-time quantitative RT-PCR after laser-assisted cell picking. Nat Med 4:1329–1333
13. Garaschuk O, Linn J, Eilers J, Konnerth A (2000) Large-scale oscillatory calcium waves in the immature cortex. Nat Neurosci 3:452–459
14. Geiger JR, Melcher T, Koh DS, Sakmann B, Seeburg PH, Jonas P, Monyer H (1995) Relative abundance of subunit mRNAs determines gating and Ca^{2+} permeability of AMPA receptors in principal neurons and interneurons in rat CNS. Neuron 15:193–204
15. Gibson UE, Heid CA, Williams PM (1996) A novel method for real time quantitative RT-PCR. Genome Res 6:995–1001
16. Hartmann J, Blum R, Kovalchuk Y, Adelsberger H, Kuner R, Durand GM, Miyata M, Kano M, Offermanns S, Konnerth A (2004) Distinct roles of $G\alpha_q$ and $G\alpha_{11}$ for Purkinje cell signaling and motor behavior. J Neurosci 24:5119–5130
17. Häusser M, Roth A (1997) Dendritic and somatic glutamate receptor channels in rat cerebellar Purkinje cells. J Physiol 501:77–95
18. Higuchi R, Fockler C, Dollinger G, Watson R (1993) Kinetic PCR analysis: real-time monitoring of DNA amplification reactions. Biotechnology (NY) 11:1026–1030
19. Jonas P, Racca C, Sakmann B, Seeburg PH, Monyer H (1994) Differences in Ca^{2+} permeability of AMPA-type glutamate receptor channels in neocortical neurons caused by differential GluR-B subunit expression. Neuron 12:1281–1289
20. Kashiwabuchi N, Ikeda K, Araki K, Hirano T, Shibuki K, Takayama C, Inoue Y, Kutsuwada T, Yagi T, Kang Y, et al (1995) Impairment of motor coordination, Purkinje cell synapse formation, and cerebellar long-term depression in GluR delta 2 mutant mice. Cell 81:245–252
21. Klein CA, Seidl S, Petat-Dutter K, Offner S, Geigl JB, Schmidt-Kittler O, Wendler N, Passlick B, Huber RM, Schlimok G, Baeuerle PA, Riethmüller G (2002) Combined transcriptome and genome analysis of single micrometastatic cells. Nat Biotechnol 20:387–392
22. Komuro H, Yacubova E, Rakic P (2001) Mode and tempo of tangential cell migration in the cerebellar external granular layer. J Neurosci 21:527–540
23. Komuro H, Yacubova E (2003) Recent advances in cerebellar granule cell migration. Cell Mol Life Sci 60:1084–1098
24. Lambolez B, Audinat E, Bochet P, Crepel F, Rossier J (1992) AMPA receptor subunits expressed by single Purkinje cells. Neuron 9:247–258
25. Liss B, Franz O, Sewing S, Bruns R, Neuhoff H, Roeper J (2001) Tuning pacemaker frequency of individual dopaminergic neurons by Kv4.3L and KChip3.1 transcription. Embo J 20:5715–5724
26. Liss B (2002) Improved quantitative real-time RT-PCR for expression profiling of individual cells. Nucleic Acids Res 30:e89
27. Mallardo M, Deitinghoff A, Müller J, Goetze B, Macchi P, Peters C, Kiebler MA (2003) Isolation and characterization of Staufen-containing ribonucleoprotein particles from rat brain. Proc Natl Acad Sci USA 100:2100–2105
28. Marandi N, Konnerth A, Garaschuk O (2002) Two-photon chloride imaging in neurons of brain slices. Pflügers Arch 445:357–365
29. Monyer H, Burnashev N, Laurie DJ, Sakmann B, Seeburg PH (1994) Developmental and regional expression in the rat brain and functional properties of four NMDA receptors. Neuron 12:529–540
30. Osada T, Uehara H, Kim H, Ikai A (2003) mRNA analysis of single living cells. J Nanobiotechnol 1:2
31. Piper M, Holt C (2004) RNA translation in axons. Annu Rev Cell Dev Biol 20:505–523
32. Plant T, Schirra C, Garaschuk O, Rossier J, Konnerth A (1997) Molecular determinants of NMDA receptor function in GABAergic neurones of rat forebrain. J Physiol (Lond) 499:47–63
33. Rasmussen R (2001) Quantification on the LightCycler. In: Meurer S, Wittwer C, Nakawara K (eds) Rapid cycle real-time PCR, methods and applications. Springer-Verlag, Berlin Heidelberg, pp 21–34
34. Rose CR, Kovalchuk Y, Eilers J, Konnerth A (1999) Two-photon Na^+ imaging in spines and fine dendrites of central neurons. Pflügers Arch 439:201–207
35. Tkatch T, Baranauskas G, Surmeier DJ (2000) Kv4.2 mRNA abundance and A-type K^+ current amplitude are linearly related in basal ganglia and basal forebrain neurons. J Neurosci 20:579–588
36. Tsuzuki K, Lambolez B, Rossier J, Ozawa S (2001) Absolute quantification of AMPA receptor subunit mRNAs in single hippocampal neurons. J Neurochem 77:1650–1659
37. Vorndran C, Minta A, Poenie M (1995) New fluorescent calcium indicators designed for cytosolic retention or measuring calcium near membranes. Biophys J 69:2112–2124
38. Whitcombe D, Theaker J, Guy SP, Brown T, Little S (1999) Detection of PCR products using self-probing amplicons and fluorescence. Nat Biotechnol 17:804–807
39. Wittwer CT, Ririe KM, Andrew RV, David DA, Gundry RA, Balis UJ (1997) The LightCycler: a microvolume multisample fluorimeter with rapid temperature control. Biotechniques 22:176–181